Using correlated tephras to refine radiocarbon-based age models, Upper and Lower Whitshed Lakes, south-central Alaska

Paul D. Zander*[,1,2], Darrell S. Kaufman[1], Nicholas P. McKay[1], Stephen C. Kuehn[3], Andrew C. G. Henderson[4]

[1]*School of Earth Sciences and Environmental Sustainability, Northern Arizona University, Flagstaff, AZ 86011-4099, USA*

[2]*Present Address: Institute of Geography & Oeschger Centre for Climate Change Research, University of Bern, Erlachstrasse 9a, 3012 Bern, Switzerland*

[3]*Department of Physical Science, Concord University, Athens, WV 24712-1000, USA*

[4]*School of Geography, Politics and Sociology, Newcastle University, Newcastle Upon Tyne, NE1 7RU, UK*

[*] *Correspondence: E-mail address: pdz2@nau.edu*

Abstract

Tephra deposits correlated between nearby lakes provide the opportunity to improve age estimates of the sediment sequences, even if the ages of the tephras are previously unknown. We explore this potential using cryptotephras and visible tephra deposits in sediment cores from Upper and Lower Whitshed Lakes near Cordova, Alaska. Each tephra was described in terms of visual stratigraphy and shard morphology, and the major-oxide glass geochemistry was analyzed. Independent age models were developed for the cores using radiocarbon ages and profiles of short-lived radioisotopes for the near-surface sediments. Four tephras were correlated between the two lakes based on the magnitude and spacing of magnetic susceptibility peaks and glass major-oxide geochemistry. These correlations confirm agreement of the age models because the independently modeled confidence intervals overlap for each correlated tephra. The stratigraphic correlations were subsequently used to improve the age models by extracting the subset of possible age-model iterations that produce similar ages for each of the four correlated tephras at the two lakes. The iterations that agree within 25 years for each correlated tephra were used to create tephra-matched age models for both lakes, which narrowed the width of the 95% confidence intervals of the age models by 3% overall and reduced the uncertainty in age estimates of the correlated tephras by 34% on average. This synchronization technique may be useful in other studies that have multiple independently dated records with confident stratigraphic correlations.

Keywords: tephrochronology, cryptotephra, age modeling, lake sediments, radiocarbon, Alaska

1. Introduction

Radiocarbon-based age models are the most common method used to date sediment cores that are less than 50,000 years old. The accuracy of these age models depends on the extent to which the constraining ages reliably represent the true timing of sedimentation. The precision of the analyses (the laboratory-reported counting error) accounts for only a small part of the overall uncertainty. More important is the extent to which the material dated actually represents the age of the down core property of interest (Howarth et al., 2013), which is difficult to evaluate without independent evidence. One indicator of the robustness of radiocarbon-based age models is whether the modeled ages of simultaneous events overlap among different cores. Previous studies have used tephra deposits as a test of age-model reliability by correlating tephras in nearby lakes and comparing their modeled ages (e.g., Krawiec et al., 2013). Even if the age of a tephra is unknown, the marker bed still provides a valuable time-line (Lowe, 2011). Dating a tephra deposit in multiple locations also improves the confidence in the age estimate of that deposit, which can then be used as a chronostratigraphic marker in future studies (Lowe, 2011; Kaufman et al., 2012).

In studies of multiple sedimentary sequences within a region, it is often desirable to synchronize the records or combine the geochronological information of multiple records. Most commonly, this is achieved through 'wiggle-matching', whereby downcore properties are aligned visually (e.g., Hoek and Bohncke, 2001; Burns et al., 2003) or quantitatively (e.g., Marwan et al., 2002; Fohlmeister, 2012). In this study, we present a novel approach that uses tephra deposits correlated between two lakes to not only check the agreement of the age models, but also to further constrain the age-depth relationship. We produced independent age models for the sedimentary sequences of Upper and Lower Whitshed Lakes located near Cordova, Alaska,

using radiocarbon and short-lived isotopes. Four tephra deposits were correlated between the two lakes based on their relative stratigraphic position, magnetic susceptibility (MS) profiles, glass geochemistry, and physical characteristics. The correlated tephras were subsequently used to select the age model runs with the closest agreement in predicting the ages of the correlated tephras. This approach allowed for a single best age estimate for each tephra to be calculated using age information from both lakes, and reduced the uncertainty range of the age-model for both sites. In addition to presenting a new approach to age modeling, we report descriptions and geochemical data from 11 tephra samples, thereby contributing to the tephrostratigraphy for the Copper River Delta region.

1.1. Study area

Upper Whitshed (60.466° N, 145.918° W) and Lower Whitshed (60.473° N, 145.923° W) Lakes are located in the foothills of the Heney Range about 12 km southwest of Cordova, Alaska, at elevations of about 30 and 3 m asl, respectively (Fig. 1). The lakes are both approximately 1 km inland from Prince William Sound on the Gulf of Alaska near Point Whitshed, from which we derive their informal names. Upper Whitshed Lake is slightly larger (1.1 x 0.2 km) than Lower Whitshed Lake (0.7 x 0.3 km). The bathymetry of Upper Whitshed Lake includes several sub-basins divided by ridges, and a maximum depth of about 15 m (Fig. 1). No bathymetric data were obtained from Lower Whitshed Lake.

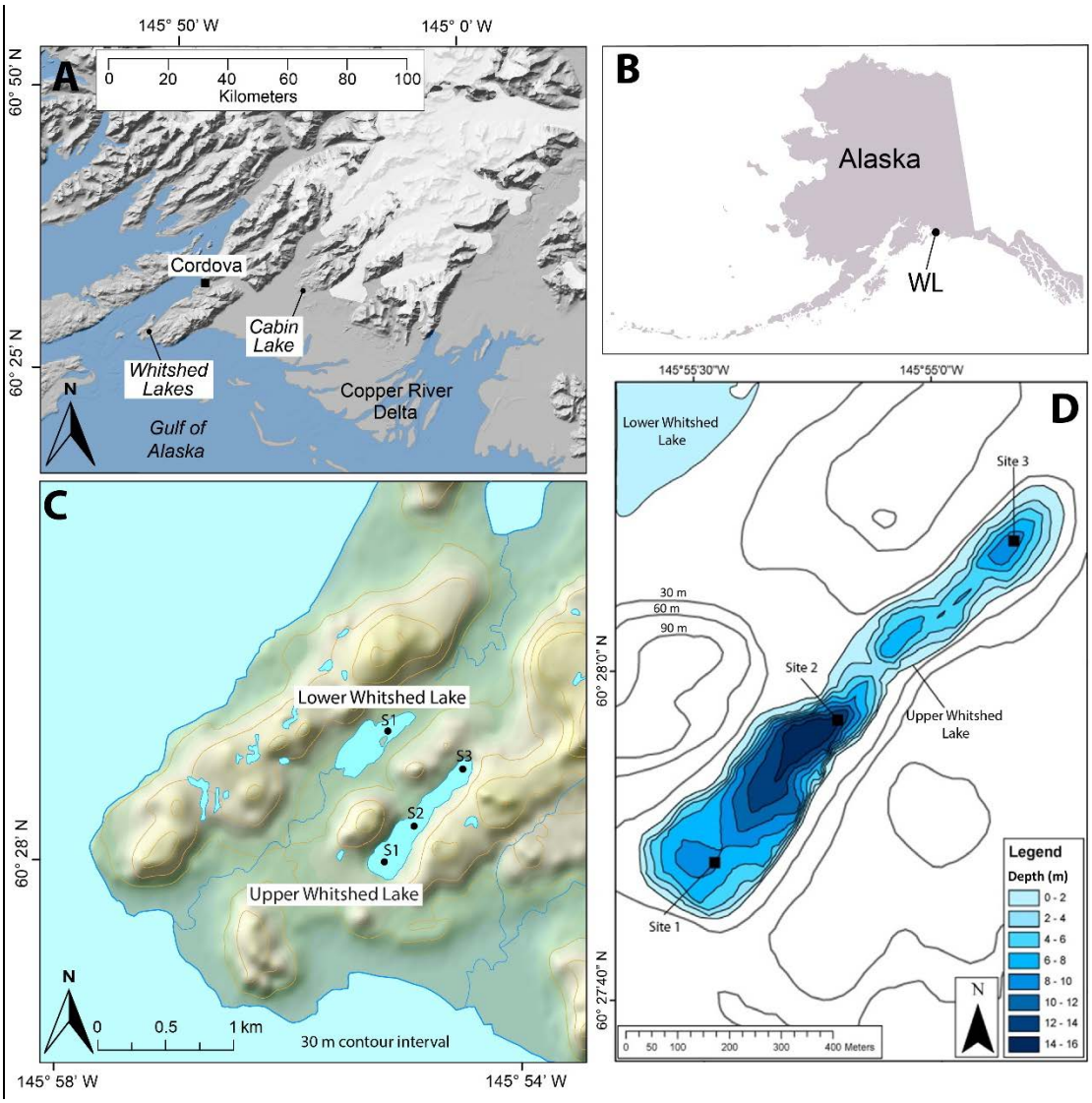

Fig 1. Location maps. (A) Copper River Delta region, showing Whitshed Lakes and other sites mentioned in text. (B) Alaska state map for reference, WL = Whitshed Lakes. (C) Whitshed Peninsula showing the two lakes with location of core sites. Topographic base from U.S. Geological Survey. (D) Bathymetry of Upper Whitshed Lake with core sites shown. Site 2 (S2) is the focus of this study from Upper Whitshed Lake.

The lakes are located near the active Alaska-Aleutian megathrust where changes in land elevation occur on multiple time scales (Garrett et al., 2015), including approximately 1.9 m of

uplift in the great Alaska earthquake of 1964 AD (Plafker, 1969). Lower Whitshed Lake received marine sediments during the Little Ice Age, and became isolated as a lacustrine basin during the 1964 event (Garrett et al., 2015). The nearest likely source volcanoes for tephras deposited in these lakes are the Aleutian Arc/Alaska Peninsula (AAAP located more than 350 km to the west and southwest) and the Wrangell Volcanic field (located more than 200 km to the northeast). Modern prevailing winds are from the southwest, making deposits from the Wrangell Volcanic field less likely. Glass compositions often distinguish AAAP (Type 1) and Wrangell (Type II) source tephras. Type I sources typically contain more FeO and TiO_2 and less Al_2O_3 and CaO (Preece et al., 1992; Fig. S1). Previous work at Cabin Lake (Zander et al., 2013), 26 km to the northeast, yielded five Holocene tephras mainly from volcanoes along the Cook Inlet of the AAAP, suggesting the same may be true of the Whitshed Lakes tephras.

2. Methods

2.1. Coring

Cores from Lower Whitshed Lake were retrieved in March 2010 from the frozen surface of the lake using a percussion corer and gravity surface corer at a single site (60.472 °N, 145.922 °W; Fig. 1). A 262-cm-long percussion core (10-WS-2) and two surface cores were collected (10-WS-1A; 165 cm and 10-WS-1B; 46 cm). Cores were retrieved from Upper Whitshed Lake in June 2011 using a percussion corer and gravity surface corer from a floating platform. To better select coring sites, Upper Whitshed Lake's bathymetry was surveyed prior to coring using a sonar unit with integrated GPS. This study focuses on site 2 (60.466 °N, 145.918 °W, Fig. 1 and 2) where the longest sedimentary sequence was recovered, including a percussion core (11-UW-2; 427 cm) and a surface core (11-UW-2A; 46 cm).

2.2. Geochronology

Age models for the sedimentary sequences from both lakes were constructed using the program "*Bacon 2.2*" (Blaauw and Christen, 2011) based on radiocarbon, lead and artificial radionuclide fallout. Organic matter for ^{14}C dating was obtained from samples of sediment 0.5-2 cm thick that were wet-sieved through a 180 µm mesh to find aquatic and terrestrial plant remains including macrofossils of *Picea*, *Tsuga*, bryophytes, and others. The samples were analyzed at the Keck Carbon Cycle AMS Facility at UC Irvine, and dates were calibrated to calendar years prior to 1950 CE (BP hereafter) using IntCal13 (Reimer et al., 2013).

Plutonium (Pu) activity profiles were analyzed in surface sediment from both lakes to locate the 1953 onset of nuclear weapons testing, and the 1963 peak fallout (Ketterer et al., 2004). Two profiles of differing resolution were analyzed on the surface cores of both lakes to ensure that the profiles captured the onset of Pu fallout and to precisely locate the depth of peak fallout. Lower Whitshed Lake surface core 10-WS-1A was sampled continuously every 0.2 cm from 0-4 cm depth for one batch. For the second batch, 1-cm-thick samples were taken continuously from 0-10 cm, and samples were taken every other cm from 10-30 cm depth. Upper Whitshed Lake surface core 11-UW-2A was sampled every 0.2 from 0-3 cm for the first batch, and every 0.5 cm continuously from 1.0-6.5 cm, with increased spacing down to 12.5 cm for the second batch. The samples were analyzed using an inductively coupled plasma mass spectrometer (ICP-MS) at Northern Arizona University.

Concentrations of ^{210}Pb, ^{241}Am and ^{137}Cs were measured on Upper Whitshed Lake surface core 11-UW-2A. Sampling was done continuously every 0.5 cm from 0-10 cm depth, and the measurements were undertaken by direct gamma assay at the Environmental Radiometric Facility at University College London. Total ^{210}Pb was determined via its gamma emissions at

46.5 keV, and ^{226}Ra by the 295 and 352 keV gamma rays emitted by its daughter isotope ^{214}Pb. Unsupported ^{210}Pb activities were calculated by subtracting ^{226}Ra activity (as supported ^{210}Pb) from total ^{210}Pb activity. Artificially produced radionuclides ^{137}Cs and ^{241}Am were measured by their emissions at 662 and 59.5 keV to determine their down-core profile, which could be ascribed to nuclear weapons testing, as for Pu. A constant-rate-of-supply (CRS) model (Appleby and Oldfield, 1978) was used to produce the ^{210}Pb age-depth relation. These analyses were not performed on sediments from Lower Whitshed Lake primarily because of expected challenges associated with a major change in the source of sediment that occurred at 1964 (marine to lacustrine transition).

2.3. Age modeling

Age models were constructed using the program *Bacon 2.2* (Blaauw and Christen, 2011), which uses a Bayesian statistical approach to construct age-depth relations through the calibrated-age probability distributions of radiocarbon dates, or other age information (i.e., marker horizons with known ages, plutonium peaks, ^{210}Pb ages). The sedimentary sequence is divided into discrete segments, and millions of Markov Chain Monte Carlo (MCMC) iterations are calculated to estimate the posterior distribution of the age-depth relation given the age control points, their uncertainties, prior estimates of the distribution of sedimentation rates and their autocorrelation, and depths where sedimentation rates are expected to change. The average of the MCMC ensemble, weighted by the log of the objective, is used as the best-fit model. Confidence intervals are calculated as the highest density range of the iterations.

The age models for both lakes were further constrained using a novel method to incorporate information provided by the tephra correlations between the two lakes. Code was developed in

MATLAB (The MathWorks, Inc.) to identify the iterations from the two independent age models that showed the closest agreement in the ages of the correlated tephras (this code is available in the supplementary material). This was done by calculating the difference between the modeled ages of each correlated tephra for each permutation of the individual models output by *Bacon 2.2* for each lake. The permutations in which the modeled age for each tephra differed by less than 25 years were selected for use in the 'tephra-matched' age models. Thus, to be included in the 'tephra-matched' age model of one lake, the ages of the four correlated tephras in the model iteration must be within 25 years of all four tephra age estimates of at least one model iteration from the other lake. The 25-year threshold was chosen to maximize the synchronization of the two age models while maintaining enough of the model iterations to calculate robust 95% confidence intervals. The choice of matching threshold has little influence on the overall outcome (see section 3.5 and Table 4).

2.3. Tephras

Tephras were located based on visual inspection of the sediment cores, and by spikes in magnetic susceptibility (MS). The tephra beds are generally lighter in color, and have higher MS than the organic-rich background lacustrine sediments. Four tephras comprise visually distinct beds that were sampled from the cores. In addition, seven zones containing cryptotephra (disseminated tephra grains that do not form visible bed) were sampled. Five of these cryptotephra samples were chosen based on notable spikes in MS, and 1-cm-thick samples were taken at the location of highest MS spikes. For two samples, age information was used as a guide to prospect for the Katmai-Novarupta ash (1912 CE), as there is evidence that fallout from the eruption reached the Cordova area (Payne and Symeonakis, 2012). Again, 1-cm-thick samples

were taken. If the tephra bed was visible on the core face, samples ranging from 0.2 to 1 cm thick were taken while avoiding adjacent lacustrine sediments. The tephra samples were named according to their depth within the individual core, which is registered to the top of the core tube rather than the composite depth below lake floor (BLF). Sediment was viewed under a petrographic microscope to confirm the presence of volcanic ash; grain size and shard morphologies were described for all tephras.

Major- and minor-element glass geochemistry for each tephra was analyzed at Concord University. For the visible tephra layers, small samples were taken (<1 cm^3) across the thickness of the visible layer. For the non-visible beds, 1-3 cm^3 of material was sampled across a 1-cm-thick interval associated with an MS peak. The cryptotephra samples were soaked in ~10% hydrogen peroxide to remove organic material, then separated by density in a lithium heteropolytungstate solution with a density of 2.5 g/cm^3. The resulting concentrates were rinsed and a portion of each was mounted following a variation of the technique described by Kuehn and Froese (2010). Samples were pipetted into holes drilled in acrylic discs, dried, embedded in epoxy, polished, and carbon coated. The samples were analyzed on an ARL SEMQ electron microprobe using the instrumentation, analytical conditions, primary and secondary standards, and normalization procedures of Zander et al. (2013) with only a change in spectrometer type for Si and Al (from wavelength-dispersive to energy-dispersive to achieve higher count rates and improved precision). Because the samples typically contained only a small number of tephra grains, two or three analyses were collected from most grains. Geochemical similarity of stratigraphically correlated tephra was determined by comparing plots of data and by using the similarity coefficient (SC) of Borchardt et al. (1972). We weight sodium oxide at 50% in the SC calculation due to larger errors associated with the measurement of this element.

3. Results

3.1. Overview of stratigraphy

Upper Whitshed Lake surface core 11-UW-2A was correlated with the percussion core 11-UW-2 based on a tephra located at 36.5 cm tube depth in the surface core and at 21.5 cm tube depth in the percussion core, indicating that the percussion core is missing the uppermost 15 cm of sediment (Fig. 2). The missing sediments are expected when using the percussion corer and necessitate the use of a composite depth scale. All depths reported hereafter are distance below the lake floor (BLF), unless otherwise stated. The 442-cm-long composite sedimentary sequence recovered from site 2 can be broken into two major units (Fig. 2). The oldest sediments below 372 cm (Unit 1) are generally massive light grayish brown (2.5Y 4/2), inorganic silty clay. Above 372 cm (Unit 2), the sediments are massive dark brown (10YR 2/2) sapropelic diatomaceous clayey silt. In addition, three tephras are visible along the core face, none thicker than 1 cm.

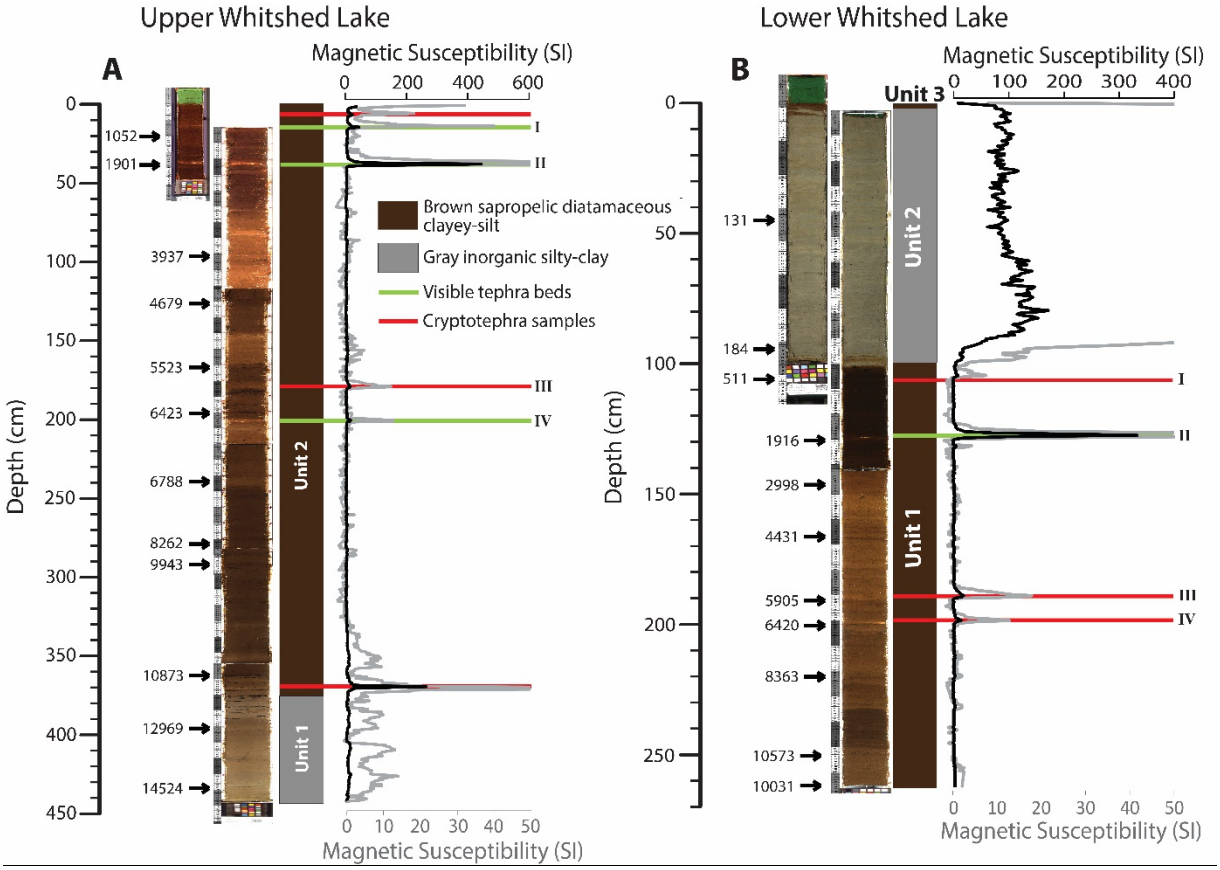

Fig. 2. Lithostratigraphy of (A) Upper Whitshed Lake cores 11-UW-2/2A, and (B) Lower Whitshed Lake cores 10-WS-2 and -1A. The linescan image of the surface core (10-WS-1A) has been stretched to approximate the depth of percussion core 10-WS-2. Horizontal bands show the location of tephra samples taken from visible beds (green) and cryptotephra (red). Tephra correlations are indicated by roman numerals (I, II, III, IV) to right of the horizontal bands. The uppermost two tephra samples from Upper Whitshed Lake (taken from 2.5 and 5 cm) are not distinguishable at this depth scale and thus are represented by a single red bar. Magnetic susceptibility is plotted on two scales to highlight smaller peaks (gray corresponds to the bottom scale). Depths are relative to the lake floor (BLF). The calibrated ages of radiocarbon samples are noted on the left of the linescan images.

The Lower Whitshed Lake sedimentary sequences (surface core 10-WS-1A and percussion core 10-WS-2) were correlated using distinctive color changes and peaks in MS, which suggest that percussion core 10-WS-2 is missing the uppermost 3.5 cm of sediment. The total recovered composite sequence is 266 cm long. All depths reported hereafter are distance below the lake floor, unless otherwise stated. The Lower Whitshed Lake composite sedimentary sequence can be divided into three major units (Fig. 2). The oldest unit (Unit 1), below 103.5 cm, is massive dark brown (10YR 2/2) sapropelic diatomaceous clayey silt. From 103.5 to 4 cm (Unit 2), the sediments are gray (5Y 4/2) inorganic clayey silt with 1- to 3-mm-thick laminations. The uppermost 4 cm (Unit 3) of sediment is brown (10YR 2/2) sapropelic diatomaceous clayey silt.

3.2. Upper Whitshed Lake age model

The concentration of ^{210}Pb from surface core 11-UW-2A increases roughly exponentially upward in the sedimentary sequence (Fig. 3; Table S1). The constant-rate-of-supply (CRS) model suggests that sedimentation rates increase from 0.3 mm/year at 8 cm up to 0.8 mm/year in the upper 2 cm of the core. Three different radionuclides produced from nuclear weapons testing were measured on surface core 11-UW-2A: $^{239+240}$Pu (Table S2), ^{137}Cs, and ^{241}Am (Table S1; Fig. 3). The onset of ^{241}Am fallout is clearly observed between 4.25 and 3.75 cm, suggesting that sediment deposited in 1953 is near 4 cm in this core. This is in agreement with the ^{210}Pb CRS model, which also suggests that 1953 is represented between 4.25 and 3.75 cm. The 1963 peak in fallout is not well defined by the radionuclide profiles, most likely a result of sediment mixing.

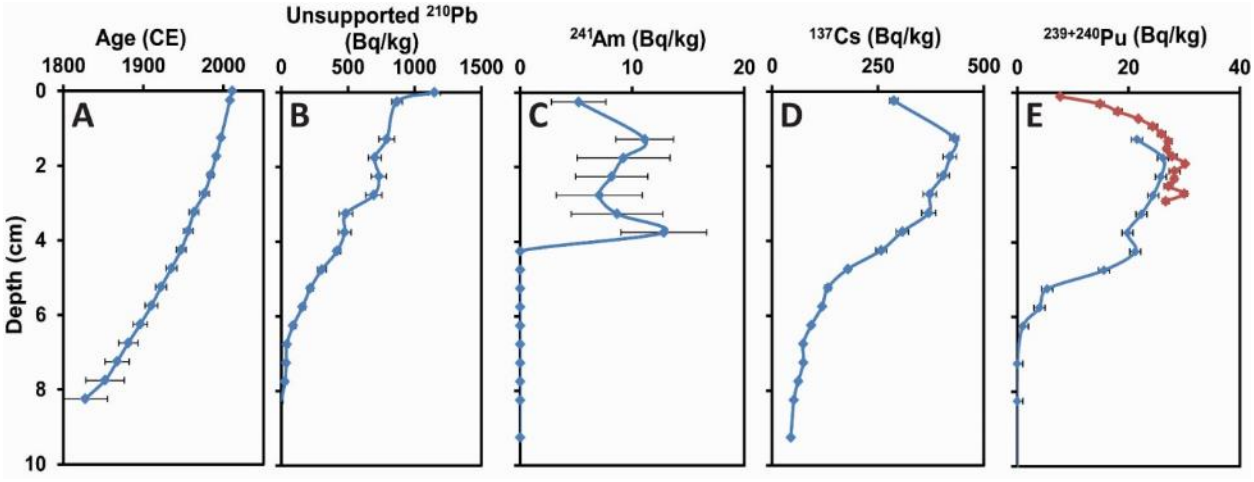

Fig. 3. Profiles of ^{210}Pb and radionuclides produced by nuclear weapons testing, Upper Whitshed Lake surface core 11-UW-2A. (A) Estimated ages from a constant-rate-of-supply model based on (B) the unsupported ^{210}Pb activity. Activities of artificial nuclides include: (C) ^{241}Am, (D) ^{137}Cs, and (E) $^{239+240}$Pu (two analytical batches shown). Bars are ± 1 SD analytical errors. Data are listed in Table S1 and S2.

The *Bacon* age model for the Upper Whitshed Lake sedimentary sequence (Table S3) was constrained by the age of the sediment surface (2011), the 1953 onset of nuclear weapons testing at 4 cm, the middle and lowest ages defined by the ^{210}Pb CRS model (1947 at 4.25 cm, and 1827 at 8.25 cm), and 13 of the 15 radiocarbon dates from the two cores at site 2 (Table 1). Two radiocarbon ages were rejected because they were not stratigraphically aligned in the sediment sequence as defined by other age information (Fig. 4). An additional radiocarbon sample from Upper Whitshed Lake has a calibrated age range that does not overlap with the 95% confidence interval of the age model. This sample has an analytical uncertainty of ± 400 years, but there was not enough evidence to reject the age, it is therefore used in the Bacon age model. Because there are no major changes in lithology to suggest a change in sedimentation rate in the Upper Whitshed Lake sequence, we used the slope of a best-fit line through the non-rejected

radiocarbon dates as the expected accumulation rate (34 years/cm) in the *Bacon* model. The default accumulation rate shape parameter (1.5) was used. The model was run with segment widths of 4 cm, a value chosen to maximize the model's resolution and smoothness without excessively long computational run times. Larger segment widths can result in an unrealistic jagged pattern of sedimentation rate changes. The output of the original, independent Upper Whitshed Lake age model can be viewed in Fig. S3.

3.3. Lower Whitshed Lake age model

Plutonium is first detected in surface core 10-WS-1A at 9.5 cm, which is interpreted as the onset of nuclear weapons testing in 1953 (Ketterer et al., 2004). Plutonium activity increases upward and peaks at 1.7 cm (Fig. 4). However, a major lithological change at 4 cm is associated with a marked change in sedimentation rate due to the isolation of the lake basin from the Gulf of Alaska (Garret et al., 2015). This change in sedimentation rate strongly influences the concentration of plutonium in the sediment, unrelated to the rate of fallout. To account for this, and to more accurately locate the peak fallout in the core, plutonium activity per unit mass (Bq kg^{-1}) was converted to a flux (i.e. activity per unit mass per year; Bq cm kg^{-1} $year^{-1}$) by multiplying by simple estimates of sedimentation rates above and below the lithological change at 4 cm. These sedimentation rates were calculated based on the onset of plutonium activity, and two radiocarbon ages obtained from within Unit 2. The peak of plutonium flux occurs at 4.5 cm, suggesting this is the approximate depth of sediment deposited in 1963 (Fig. 4). Because this peak is essentially defined by the sharp change in sedimentation rate superposed on an upward-increasing trend, there is some uncertainty about the placement of the peak in fallout. However, the sedimentation rate change associated with a marine-to-lacustrine transition was most likely

caused by uplift during the 1964 Great Alaska Earthquake (Garrett et al., 2015), suggesting that 1964 is represented near 4 cm depth.

The age model for the sedimentary sequence recovered from Lower Whitshed Lake (Table S4) was based on the age of surface core, the onset and peak of nuclear weapons testing as recorded in the plutonium profile, and 11 radiocarbon dates. The two basal ages from Lower Whitshed Lake are out of stratigraphic order, but it is difficult to assess which is more accurate, so both are included. Three different prior estimates of sedimentation rates were input into the *Bacon* program based on changes in stratigraphy: (1) from the base of the sequence (265.5 cm) to 103.5 cm, an expected sedimentation rate of 65 years/cm was used, based upon radiocarbon ages in this segment; (2) between 103.5 and 4 cm, a sedimentation rate of 3 years/cm was used, based upon two radiocarbon dates and the 1953 onset of nuclear weapons testing at 9.5 cm; and (3) from 4 to 0 cm, a rate of 11 years/cm was based on an extrapolation that assumed the sedimentation rate from 9.5 to 4 cm was consistent with the rest of Unit 2, and that the sedimentation rate shifted from 4 cm to the core top. The default accumulation shape parameter (1.5) was used for each of these segments. A segment width of 2 cm was selected to maximize the resolution and smoothness of the model output without excessively long run times. The output of the original, independent Lower Whitshed Lake age model can be viewed in Fig. S4.

Table 1

Radiocarbon ages from Upper and Lower Whitshed Lake sediment cores.

Lab ID (UCIAMS)	Top tube depth (cm)	Bottom tube depth (cm)	Top depth BLF (cm)	Bottom depth BLF (cm)	^{14}C age (yr BP)	Calibrated age (BP) [b]	Material
Upper Whitshed Lake (surface core 11-UW-2A and percussion core 11-UW-2)							
107549[a]	19.5	21.5	19.5	21.5	1140 ± 50	1055 ± 100	Non-specific plant remains, *Daphnia* ephippia
98669	23.0	24.0	38.0	39.0	1815 ± 50	1750 ± 91	Two *Tsuga* needles, one *Picea* needle, wood fragments
104760	81.0	82.0	96.0	97.0	3625 ± 35	3937 ± 45	Terrestrial leaf fragments, small wood fragments
107547	111.0	112.0	126.0	127.0	4135 ± 20	4679 ± 112	Pressed non-specific organics, bryophyte twig, leafy material
104761[c]	130.0	131.0	145.0	146.0	2460 ± 20	2593 ± 118	*Picea* needles, bryophyte twig, *Tsuga* needle, bryozoan statocyst, non-specific organics
107548	151.5	152.5	166.5	167.5	4765 ± 20	5523 ± 54	Bryophytes, terrestrial leaves, sedge (Cyperaceae) achene
100080	180.5	181.5	195.5	196.5	5640 ± 30	6423 ± 34	Leaf fragment, stem fragments - terrestrial
104762	224.0	225.0	239.0	240.0	5960 ± 30	6787 ± 51	Small terrestrial leaf fragments
121202	263.5	264.5	278.5	279.5	7450 ± 20	8263 ± 59	Large plant spike
104763	276.0	278.0	292.0	293.0	8840 ± 400	9943 ± 509	Terrestrial leaf fragments
128102[c]	279.5	280.5	294.5	295.5	8030 ± 30	8907 ± 109	Leaf fragment
121203	302.5	304.5	317.5	319.5	6830 ± 30	7660 ± 30	Chitin, leaves, twigs, stems, seed capsules
100081	347.0	348.0	362.0	363.0	9530 ± 60	10870 ± 179	Leaf fragments and bryophyte twigs
104764	380.5	381.5	395.5	396.5	11070 ± 40	12940 ± 74	Terrestrial leaf fragments (from small shrub), lots of bryophyte twigs
100082	418.0	420.0	433.0	435.0	12430 ± 100	14560 ± 262	Bryophyte, unidentifiable fragments, Ericaceae seed, leaf fragments
Lower Whitshed Lake (percussion core 10-WS-2)							
76307	44.5	45.5	48.0	49.0	135 ± 20	134 ± 127	Hemlock (*Tsuga*) needle fragments, bryophyte capsules
82286	94.0	95.0	97.5	98.5	175 ± 20	184 ± 130	*Tsuga* needles, alder (*Alnus*) leaf fragments, conifer seed, wood fragments
76308	105.5	106.5	109.0	110.0	455 ± 15	511 ± 6	*Picea* needles and twigs, *Tsuga* needle
82287	129.0	130.0	132.5	133.5	1970 ± 15	1915 ± 20	Two *Picea* and one *Tsuga* needles, conifer seed wing, conifer seed fragment
82288	146.0	147.0	149.5	150.5	2875 ± 20	2996 ± 49	Conifer wing fragment, *Picea* seed and needles, chitin from aquatic insects

82289	166.0	167.0	169.5	170.5	3960 ± 30	4431 ± 54	All aquatic material, caddisfly case
82290	190.0	192.0	193.5	195.5	5130 ± 20	5906 ± 14	All aquatic chitin
82291	200.0	201.0	203.5	204.5	5635 ± 20	6420 ± 21	*Cladocera* chitin, terrestrial leaf vein, alder leaf, moss fragments
82292	221.0	221.0	224.5	224.5	7525 ± 20	8363 ± 14	All aquatic; chitin, chironomid head fragments, non-specific plants (moss branches?)
76309	250.0	251.0	253.5	254.5	9355 ± 25	10570 ± 63	Unspecified leaf fragments
82293	261.0	263.0	263.5	266.5	8875 ± 30	10030 ± 116	Terrestrial leaf fragments, aquatic chitin, *Najas* (floating leaf aquatic plant)

[a] Age from surface core 11-UW-2A, all others are from percussion cores
[b] Median probability age from Calib 7.0 (Reimer et al., 2013); ± = one-half of 1σ range
[c] Rejected age

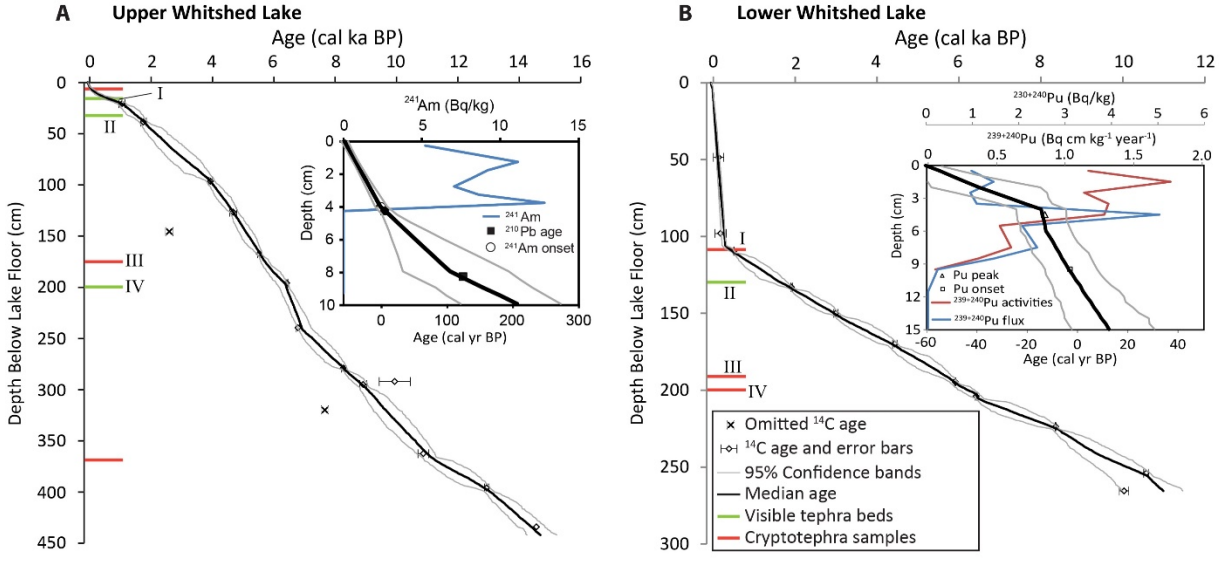

Fig. 4. Age models for sediment cores from (A) Upper and (B) Lower Whiteshed Lakes. Insets show uppermost portions of age models in detail and radionuclide profiles used to constrain ages near the surface. Tick marks along the depth scale show the locations of tephra samples, green indicates samples taken from visible beds, and red indicates samples of cryptotephra. Numerals (I, II, III, IV) adjacent to these tick marks indicate the correlations between the lakes. The uppermost two tephra samples from Upper Whitshed Lake (taken from 2.5 and 5 cm) are not distinguishable at this depth scale and thus are represented by a single red bar. Error bars for ^{14}C

ages are 1σ calibrated age ranges (data listed in Table 1). Complete input and outputs for these age models are in Tables S3, S4, S6, and S7.

3.4. Tephrostratigraphy

A total of 11 tephra samples were collected from the two lakes, seven from Upper Whitshed Lake and four from Lower Whitshed Lake (Table 2 summarizes the tephrostratigraphy of the two lakes). Three of the Upper Whitshed Lake samples were collected from visible beds and the other four samples were collected from zones of disseminated cryptotephra with high MS values (Table 3; Fig. 3). Only one tephra was visible in the core from Lower Whitshed Lake, while the other three samples were taken from zones of disseminated tephra indicated by MS peaks. All of the samples from visible beds and all but two of cryptotephra samples yielded distinct geochemical populations (Fig. 5 and 6). Overall, the glass chemistries are indicative of primarily AAAP (Type I) sources, although some of the data overlap the boundary between Type I and Type II compositional fields (Fig. S2).

The glass geochemistry supports stratigraphic correlations of four tephra beds between the two lakes: 10-WS-2-1-104.5 with 11-UW-2A-13, 10-WS-2-127.5 with 11-UW-2A-36.5, 10-WS-2-189 with 11-UW-2-163.5, and 10-WS-2-198.5 with 11-UW-2-2-185 (note that tephra sample IDs use tube segment numbers and depths, and not composite depth BLF). Table S5 includes the complete geochemical results for Whitshed Lakes tephras. Ages reported in this section (3.4) are based on the independently produced age models without the tephra-matching routine to refine the models; this is done in order to present the original chronological uncertainty associated with these deposits prior to correlation.

345 Two samples were analyzed in an attempt to identify glass shards from the 1912 eruption of
346 Novarupta, which is interpreted to have likely deposited tephra near Cordova by Payne and
347 Symeonakis (2012). The eruptive material of Novarupta was derived from a zoned magma
348 chamber, and has a wide variety of compositions, ranging from 58.5–78.0% SiO_2 (Hildreth,
349 1987). Sample 11-UW-2A-2.5 (Concord University ID: CU1286, 1975 ± 7 CE) is not associated
350 with an MS peak and is too young to contain a primary deposit from Novarupta. 11-UW-2A-5
351 (CU1160, 1926 ± 22 CE) is associated with a minor MS peak (3.3 SI units) and has a modeled
352 age that overlaps 1912 CE. Sample 11-UW-2A-2.5 contains two well-defined major populations
353 (Fig. 6): (1) a heterogeneous population with a SiO_2 range of 58–75 wt%, and (2) a
354 homogeneous high silica population with SiO_2 ~78 wt%. The latter is an excellent match (SC
355 0.97) for the high silica end-member composition of Novarupta 1912 and likely represents
356 reworked material from the Novarupta eruption. The heterogeneous population, however, plots
357 away from the lower silica components of the 1912 eruption (Table S5) and likely represents a
358 different event. Sample 11-UW-2A-5 (CU1160) contains the same two populations, although the
359 ~78 wt% SiO_2 population is represented only by a single analysis (fewer shards were analyzed in
360 this sample, so this may be due to sampling bias).
361 11-UW-2A-13 (CU1161, 464 ± 325 BP) and 10-WS-2-104.5 (CU1278, 382 ± 107 BP) are
362 correlated based on their independently modeled ages, similar-magnitude MS peaks, and glass
363 geochemistry (SC = 0.97). Both samples contain mainly andesitic glass (Fig. 5), with a
364 secondary population of more silicic glass (33% of grains in 11-UW-2A-13; 19% in 10-WS-2-
365 104.5). The geochemical composition of most of these shards overlap with the distribution
366 defined by population 1 in 11-UW-2A-2.5 (CU1286) described above.

11-UW-2A-36.5 (CU1162, 1654 ± 196 BP) and 10-WS-2-127.5 (CU1149, 1748 ± 189 BP) are correlated based on their independently modeled ages, similar physical characteristics, high MS values, and glass geochemistry (SC = 0.94). Both samples contain rhyolitic glass with little compositional variability. The geochemistry of this sample is indistinguishable (SC 0.97; Table S5) from sample 10-CB-1-C-102 (CU1148, 1303 ± 55 BP) at Cabin Lake (Zander et al., 2013), but the ages differ, suggesting either that the two lakes contain tephras of different eruptions from the same source, or that the Cabin Lake age may be somewhat inaccurate.

The stratigraphic levels represented by samples 11-UW-2-163.5 (CU1157, 5863 ± 229 BP) and 10-WS-2-189 (CU1150, 5498 ± 291 BP) are correlated based on their independently modeled ages and distinctive MS stratigraphy in this part of the core. The glass geochemistry of these samples is relatively scattered ranging from 59-80% silica. Overall the geochemical data of the samples overlap, but there are significant differences. Sample 11-UW-2-163.5 contains a mixture of andesitic/dacitic glass shards and fewer rhyolitic shards. Sample 10-WS-2-189 contains a mixture of mainly rhyolitic glass shards with few andesitic/dacitic shards. The high silica modes yield an SC value of 0.83, but this is based on only six data points from 11-UW-2-163.5. These samples may include reworked material from multiple eruptions, and this interpretation is supported by evidence of subtle rounding of glass shards in 11-UW-2-163.5.

11-UW-2-185 (CU1158, 6442 ± 140 BP) and 10-WS-2-198.5 (CU1151, 6246 ± 199 BP) are correlated based on independently modeled ages, similar magnitude MS peaks, and glass geochemistry (SC = 0.93). Both samples contain homogeneous rhyolitic glass.

11-UW-2-355 (CU1159, 11370 ± 410 BP) contains a bimodal population of dacitic/rhyolitic glass. No equivalent is found in the Lower Whitshed Lake cores because it is older than the oldest recovered sediments from the lower lake. This bed may correlate with sample 11-CB-4-4-

269 (CU1154, 10,636 ± 195 BP) at Cabin Lake (Zander et al., 2013); both samples contain the same bimodal compositional distribution (Table S5). The age estimates differ slightly, but the age control for the Cabin Lake sample is poor, allowing for the possibility of a correlation.

Table 2

Tephras in sediment of Upper and Lower Whitshed Lakes, with age estimates based on independent and tephra-matched age models and descriptions of tephra beds (if visible) and shard morphology.

Sample ID	Concord University ID	Depth BLF (cm)	Thickness (cm)[a]	Independently modeled age[b]	Tephra-matched age[b]	SC[c]	Description
Upper Whitshed Lake							
11-UW-2A-2.5	CU1286	2.5	-	1975 ± 7 CE	1975 ± 6 CE	-	Rare frothy pumice and angular blocky shards smaller than 50 µm.
11-UW-2A-5	CU1160	5	-	1926 ± 20 CE	1926 ± 20 CE	-	Rare frothy pumice and angular blocky shards smaller than 60 µm.
11-UW-2A-13	CU1161	13	0.2	464 ± 325 BP[d]	393 ± 103 BP	0.97 (I)	Correlated with 10-WS-2-104. Light tan bed with sharp contacts. Bubble-walled shards up to 130 µm are dominant with frothy pumice and blocky shards also present.
11-UW-2A-36.5	CU1162	36.5	0.5	1654 ± 196 BP	1719 ± 160 BP	0.94 (II)	Correlated with 10-WS-2-127.5. Light tan bed with sharp contacts. Bubble-walled shards up to 200 µm are most common. Also present are equant blocky shards, frothy pumice with elongate vesicles, and needle shaped shards.
11-UW-2-163.5	CU1157	178.5	-	5863 ± 229 BP	5791 ± 135 BP	0.83[e] (III)	Correlated with 10-WS-2-189. Dominantly equant blocky shards up to 120 µm, with some frothy pumice, and occasional bubble-walled shards.
11-UW-2-185	CU1158	200	1.0	6442 ± 140 BP	6397 ± 171 BP	0.93 (IV)	Correlated with 10-WS-2-198.5. Medium brown bed with diffuse contacts. Mainly equant blocky shards up to 130 µm. Bubble-walled shards and frothy pumice are also present.
11-UW-2-355	CU1159	370	-	11370 ± 410 BP	11310 ± 456 BP	-	Dominantly equant blocky shards, and some elongate shards, which may be bubble-walled shards. The largest shards are 180 µm.
Lower Whitshed Lake							
10-WS-2-104.5	CU1278	108	-	382 ± 107 BP	393 ± 103 BP	0.97 (I)	Correlated with 11-UW-2A-13. Mainly bubble-walled shards and tricuspate forms. Frothy pumice with elongate vesicles and blocky shards are also present. The largest shards are 120 µm

10-WS-2-127.5	CU1149	131	0.5	1748 ± 189 BP	1719 ± 160 BP	0.94 (II)	Correlated with 11-UW-2A-36.5. Light tan bed with sharp contacts. Bubble-walled shards are most common. Equant and tabular blocky shards, elongate needle shaped shards, and frothy pumice with elongate vesicles are also present. The largest shards are 180 µm.
10-WS-2-189	CU1150	192.5	-	5703 ± 233 BP	5791 ± 135 BP	0.83[e] (III)	Correlated with 11-UW-2-163.5. Mainly blocky equant shards, with tabular blocky shards and bubble-walled shards also common. Frothy pumice is rare. The largest grains are 140 µm.
10-WS-2-198.5	CU1151	202	-	6246 ± 199 BP	6397 ± 171 BP	0.93 (IV)	Correlated with 11-UW-2-185. Blocky shards are the most common, with both equant and tabular forms. Bubble walled shards are also common. Elongate shards and frothy pumice are rare. The largest grains are 110 µm.

[a] "—" = tephra not visible on the core face; sample thickness was 1 cm for these cryptotephra samples

[b] error range is equal to half the width of the 95% confidence interval

[c] SC = Similarity Coefficient (Borchardt et al., 1972); correlated samples are noted by numerals in parenthesis

[d] BP = cal yr before 1950 CE

[e] SC value from high-silica modes of 10-WS-2-189 (major population) and 11-UW-2-163.5 (secondary population)

Table 3

Summary of normalized major-element compositions of tephra glass from Upper and Lower Whitshed Lakes. Complete data in Table S5. Outlying data points are generally excluded here.

Sample[a]		SiO_2	TiO_2	Al_2O_3	FeO_t[b]	MnO	MgO	CaO	Na_2O	K_2O	P_2O_5	Cl	Total	*n*[c]
Upper Whitshed Lake														
11-UW-2A-2.5 (CU1286[d])														
Lower silica end member of mixing trend	Mean	59.79	1.20	16.01	7.91	0.19	2.75	6.13	3.81	1.80	0.29	0.12	100	20
	StDev	1.05	0.07	0.32	0.64	0.03	0.25	0.40	0.49	0.17	0.05	0.02		
Higher silica end member of mixing trend	Mean	74.57	0.32	13.92	1.56	0.07	0.39	1.82	4.15	3.02	0.04	0.17	100	8
	StDev	0.41	0.02	0.31	0.10	0.02	0.02	0.23	0.27	0.19	0.03	0.02		
Highest silica population	Mean	78.06	0.15	12.32	1.20	0.04	0.10	0.73	4.03	3.19	0.02	0.21	100	14
	StDev	0.45	0.02	0.18	0.12	0.03	0.01	0.05	0.36	0.09	0.03	0.02		
11-UW-2A-5 (CU1160)														
Higher silica end member	Mean	74.52	0.31	14.15	1.54	0.08	0.37	1.78	4.21	2.86	0.07	0.15	100	6
	StDev	0.30	0.03	0.24	0.09	0.03	0.03	0.11	0.21	0.24	0.04	0.03		
Highest silica (similar to Novarupta/CU1286)		77.81	0.15	12.28	1.06	0.09	0.09	0.81	4.39	3.13	0.01	0.22	100	1
Overall Average	Mean	70.98	0.51	14.62	2.94	0.11	0.82	2.69	4.45	2.62	0.12	0.17	100	11
	StDev	5.34	0.31	1.09	2.04	0.05	0.72	1.44	0.41	0.41	0.08	0.06		
11-UW-2A-13 (CU1161)														
Low-silica mode	Mean	60.34	1.16	16.15	7.63	0.23	2.66	5.56	4.02	1.85	0.30	0.12	100	12
	StDev	1.46	0.06	0.22	0.67	0.04	0.35	0.58	0.33	0.18	0.04	0.01		
High-silica mode	Mean	70.93	0.64	14.64	3.07	0.12	0.57	2.02	4.63	3.14	0.12	0.16	100	6
	StDev	2.66	0.23	1.13	0.74	0.03	0.37	0.93	0.87	0.52	0.08	0.02		
11-UW-2A-36.5 (CU1162)	Mean	74.51	0.36	13.94	1.65	0.09	0.37	1.74	4.19	2.95	0.07	0.18	100	13
	StDev	0.31	0.05	0.25	0.11	0.03	0.03	0.11	0.32	0.12	0.03	0.02		
11-UW-2-163.5 (CU1157)														
Low-silica mode	Mean	65.37	1.19	15.08	6.04	0.12	1.14	3.79	4.17	2.53	0.32	0.32	100	15
	StDev	2.72	0.60	0.80	2.40	0.07	0.54	0.94	1.04	0.51	0.23	0.13		
High-silica mode	Mean	77.36	0.29	12.84	1.33	0.04	0.28	1.05	3.27	3.29	0.03	0.26	100	6
	StDev	1.61	0.03	0.36	0.23	0.02	0.11	0.99	1.60	1.78	0.01	0.09		

11-UW-2-185 (CU1158)	Mean	76.90	0.31	12.80	1.59	0.06	0.31	1.76	4.17	1.92	0.04	0.17	100	14
	StDev	0.50	0.03	0.24	0.08	0.02	0.03	0.10	0.34	0.08	0.02	0.02		
11-UW-2-355 (CU1159)														
Low-silica mode	Mean	70.19	0.60	15.00	3.26	0.12	0.92	2.92	4.37	2.32	0.16	0.18	100	11
	StDev	0.70	0.03	0.32	0.16	0.03	0.09	0.31	0.34	0.09	0.02	0.03		
High-silica mode	Mean	75.63	0.32	13.31	1.69	0.07	0.37	1.52	4.20	2.61	0.05	0.16	100	4
	StDev	0.56	0.01	0.08	0.08	0.01	0.01	0.04	0.55	0.06	0.05	0.01		
Lower Whitshed Lake														
10-WS-2-104.5 (CU1278)														
Low-silica mode	Mean	60.26	1.15	15.94	7.45	0.22	2.63	5.81	4.26	1.88	0.29	0.13	100	15
	StDev	1.45	0.06	0.25	0.73	0.04	0.36	0.59	0.50	0.24	0.04	0.04		
High-silica mode	Mean	76.64	0.23	12.80	1.11	0.09	0.21	1.19	4.32	3.25	0.04	0.15	100	3
	StDev	0.27	0.01	0.16	0.01	0.03	0.01	0.09	0.43	0.07	0.20	0.01		
10-WS-2-127.5 (CU1149)	Mean	74.55	0.33	13.90	1.55	0.08	0.38	1.64	4.33	3.05	0.06	0.16	100	15
	StDev	0.43	0.02	0.31	0.07	0.02	0.02	0.09	0.44	0.09	0.03	0.03		
10-WS-2-189 (CU1150)														
Low-silica mode	Mean	63.36	0.92	15.81	5.51	0.31	2.50	4.57	4.02	2.12	0.72	0.21	100	3
	StDev	5.36	0.47	0.62	3.50	0.19	2.40	1.48	0.31	0.89	0.74	0.03		
High-silica mode	Mean	76.85	0.32	12.71	1.40	0.05	0.13	0.76	3.32	4.24	0.06	0.21	100	18
	StDev	1.28	0.16	0.58	0.30	0.02	0.08	0.45	0.68	1.20	0.07	0.11		
10-WS-2-198.5 (CU1151)	Mean	76.91	0.29	12.62	1.49	0.04	0.33	1.84	4.34	1.94	0.04	0.19	100	15
	StDev	0.36	0.03	0.31	0.08	0.02	0.02	0.15	0.44	0.04	0.02	0.02		

[a] Samples are listed in order of age (within each lake) with youngest at top
[b] FeO_t is total iron oxide as FeO
[c] *n* = number of analyses
[d] CUXXXX = Concord University sample IDs

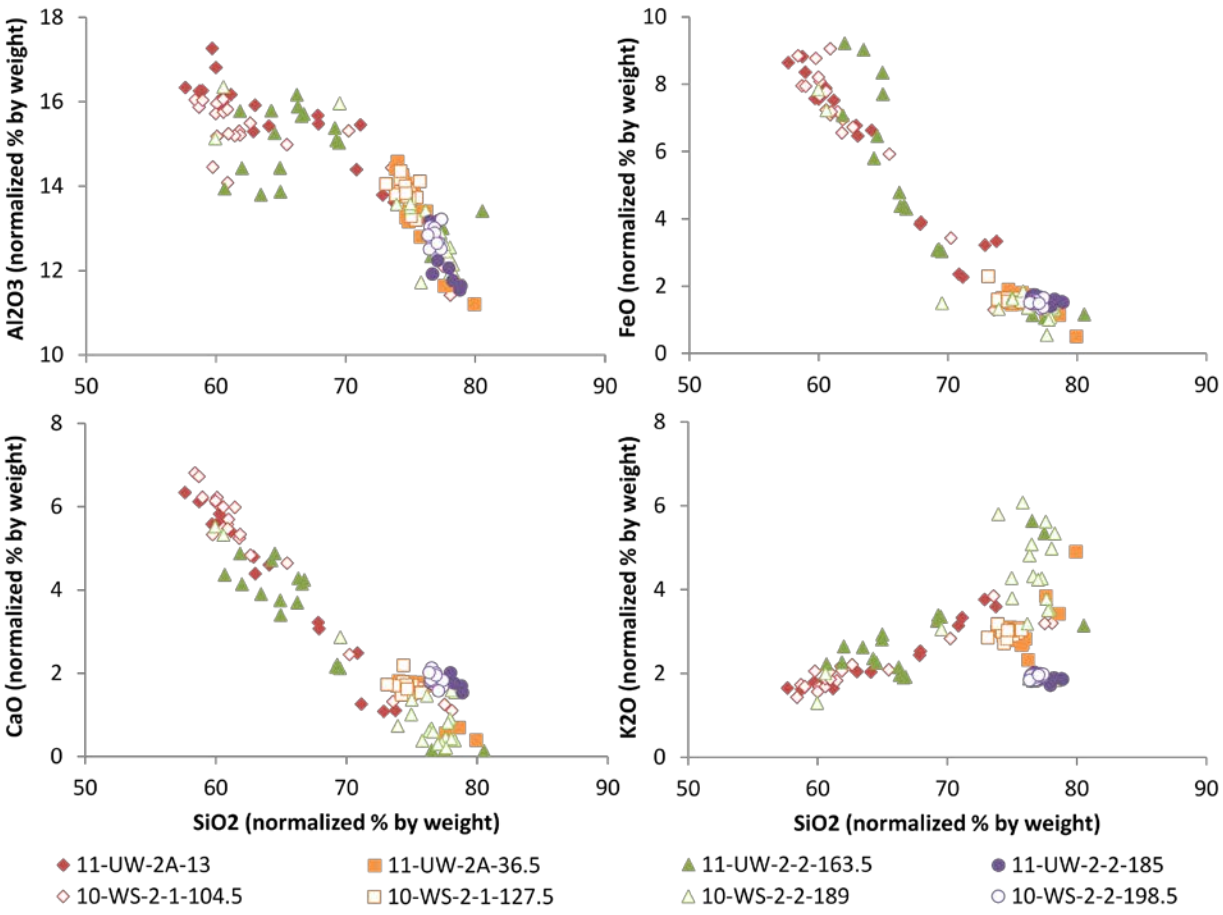

411

412 **Fig. 5.** Bivariate plots of glass geochemistry (all analyses, excluding outliers) of the tephras that
413 are stratigraphically correlated between the two lakes. Plot symbols are coded such that
414 correlative tephras have the same shape and color, but data from Upper Whitshed Lake are
415 represented by filled symbols; symbols from Lower Whitshed Lake have no fill. Data are listed
416 in Table S5.

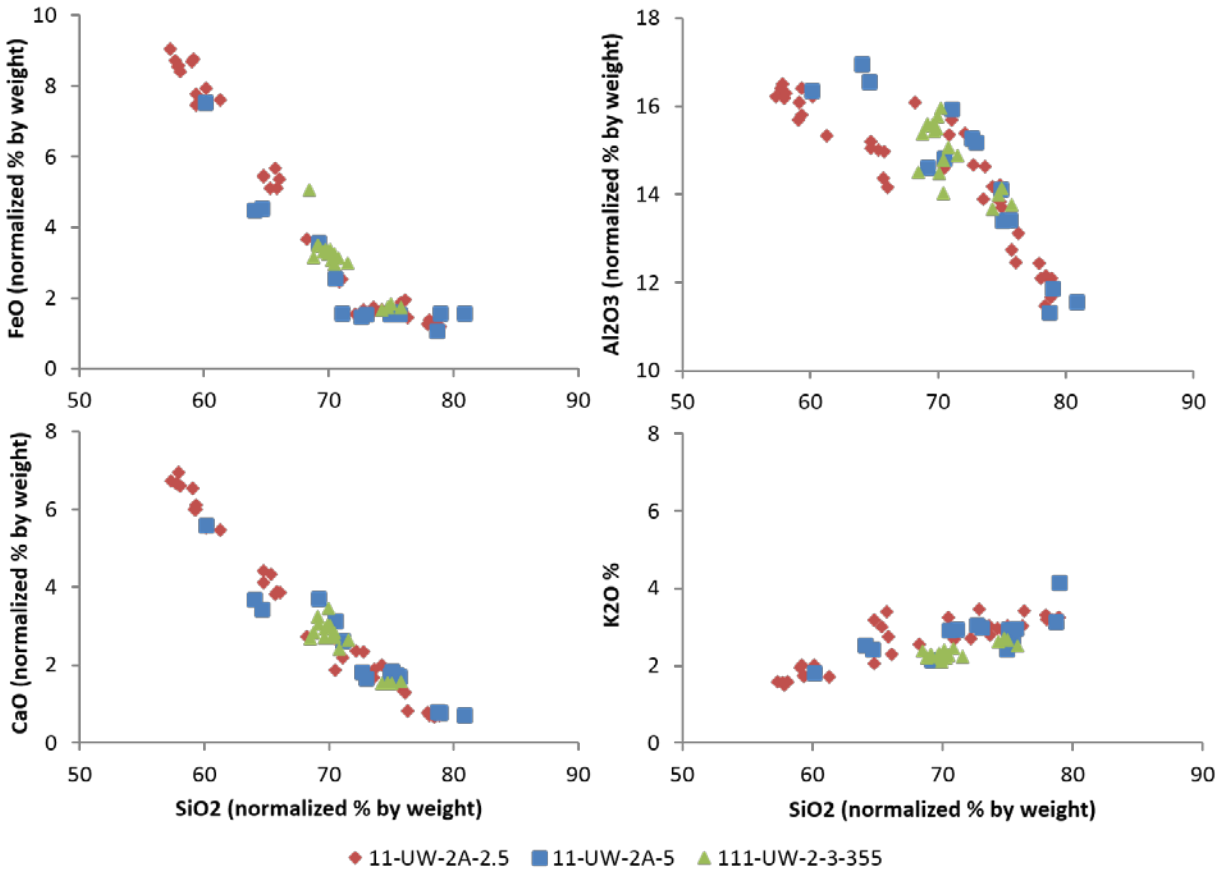

417

418 **Fig. 6.** Bivariate plots of glass geochemistry of the tephras from Upper Whitshed Lake that were
419 not found in Lower Whitshed Lake. Samples 11-UW-2A-2.5 and 11-UW-2A-5 are from beds of
420 disseminated cryptotephra. Complete data and additional plots are included in Table S5.

421

422 *3.5. Improved tephra-matched age models*

423 Four tephras were correlated between the sedimentary sequences of Upper and Lower
424 Whitshed Lakes (refer to section 3.4), and the independently derived age estimates of these
425 tephras agree within the 95% confidence intervals of the age models in all four cases (Table 2).
426 These correlations were used to select age-depth model iterations from the *Bacon* output in
427 which the ages of all four tephra differed by less than 25 years when compared between the two
428 lakes. The *Bacon* output includes over 4000 ensemble members for each lake, each of which

represents a unique fit to the probability density functions of the calibration of the ^{14}C ages for each lake. This yielded over 17 million possible permutations of the outputs from both lakes, and only 663 permutations (365 unique iterations from Upper Whitshed Lake, and 394 unique iterations from Lower Whitshed Lake) met the criteria of predicting the ages of all four of correlated tephra to be no more than 25 years apart in the two lakes. This subset of ensemble members comprises the primary age models for this study (Tables S6 and S7 contain the complete age estimates at 0.5 cm scale).

Overall, the 'tephra-matched' age models are very similar to the independent models: the average absolute deviation in median age between independent models and tephra-matched models is roughly 18 years for both lakes. Larger differences occur near the four tie-points. The tephra-matched age models reduce the overall uncertainty range of the age models modestly (by about 3%). The average width of the 95% confidence interval) decreased from 582 to 567 years, and from 416 to 398 years in Upper and Lower Whitshed Lakes, respectively (Table 4).

For each of the four tephras that were correlated between the two lakes, a single best-age estimate was calculated using the combined outputs of the age models for both lakes. All 758 model iterations that met the criteria were combined and used to calculate the median and 95% confidence intervals for the four tephras. This reduced the width of the 95% confidence intervals of these tephras by 33% on average compared to the independent age models from the two lakes (Table 2). The combined ages are used for the four tephras for the remainder of the study.

Table 4

Comparison of different tephra matching criteria and the resulting age uncertainty for each lake, and for the four tephras correlated between the lakes.

Tephra-match criterion (years)	# of matched permutations[a]	# of Upper Whitshed iterations	# of Lower Whitshed iterations	Upper Whitshed average 95% confidence range (years)	Lower Whitshed average 95% confidence range (years)	Average 95% confidence range for correlated tephra (years)
Independent	-	4129	4118	582	416	420
15	90	84	83	565	409	259
25	663	365	394	567	398	284
50	11933	1295	1867	561	402	324
100	205541	2828	3752	563	405	400

[a] out of 17,003,222 permutations

4. Discussion

4.1. Advantages and limitations of tephra-matched age models

The tephra and stratigraphic correlations between Upper and Lower Whitshed Lakes show that the radiocarbon-based age models are in good agreement. The novel approach in this study used the output of a Bayesian, Monte Carlo-based age-modeling routine (*Bacon*) to synchronize and further constrain the age models by selecting the individual ensemble members that show reasonable agreement between the two sedimentary sequences. This method could be applied to any sequences with well-correlated marker beds; however, some overlap between the confidence intervals of the ages of correlated markers is needed to generate a sufficient number of iterations with matched ages. Here we have synchronized two sequences, but the same technique could be used with multiple records. A potential source of error in this technique is correlating events that appear to be synchronous, but actually are not. One example would be correlating tephra material that is geochemically similar but might be from different eruptions of the same volcanic system. In this study, the distinct spacing and magnitude of the MS profile in conjunction with the relatively well-dated sequences make the likelihood of such an error low.

The uncertainty ranges of ages produced by this method depend somewhat on the cut-off value used to select the runs (i.e. the matching criterion). The sensitivity of the resulting age uncertainty to the choice of matching criterion was assessed by culling the age-model ensemble using different cut-off values. The results show that the matching-criterion value has a small impact on the overall uncertainty of the age models, and that using broader matching criteria can unexpectedly result in a slightly narrower average confidence interval (Table 4). This result can be explained by the reduced weight of outlying age estimates when a greater number of iterations are included in the ensemble. The age uncertainties for the correlated tephras are more strongly dependent on the choice of matching criterion and therefore are not strictly objective. In this study, iterations with predicted ages of the correlated tephras that were less than 25 years apart between the two lakes were selected for the tephra-matched age model. This cut-off was chosen as a compromise between the competing goals of matching the age models as closely as possible, while not being so restrictive that the number of acceptable iterations would be too small for a robust estimate of the 95% confidence interval. While a longer run time could generate more age-depth iterations, and the potential to use a more restrictive matching criterion, 25 years is represented by about 0.5 cm of sediment on average for Unit 1 in Lower Whitshed Lake, which is near the limit of the accuracy of the depth scales for our core samples. Like all age-modeling routines, the selection of the goodness-of-fit criterion is somewhat subjective and dependent on what the data allow. This method ensures that the two records are synchronized at four different tie-points, but beyond those depths it is not possible to ascertain to what degree the age models agree or diverge.

The tephra-matched age models improve on the independently produced age models by integrating geochronological information from more than one site. This is supported by

correlations between biogenic silica (BSi) records (Zander, 2015) from the two lakes (Fig. 7 and 8). An average correlation coefficient of 0.38 was calculated for the BSi records of the two lakes using the 365 tephra-matched iterations from Upper Whitshed Lake and a random selection of 365 iterations from the Lower Whitshed Lake tephra-matched model. This improves upon the 0.34 average correlation coefficient calculated using 365 randomly selected iterations from the independent age models. Although the difference is small, it is significant ($p < 0.0001$) based on a t-test.

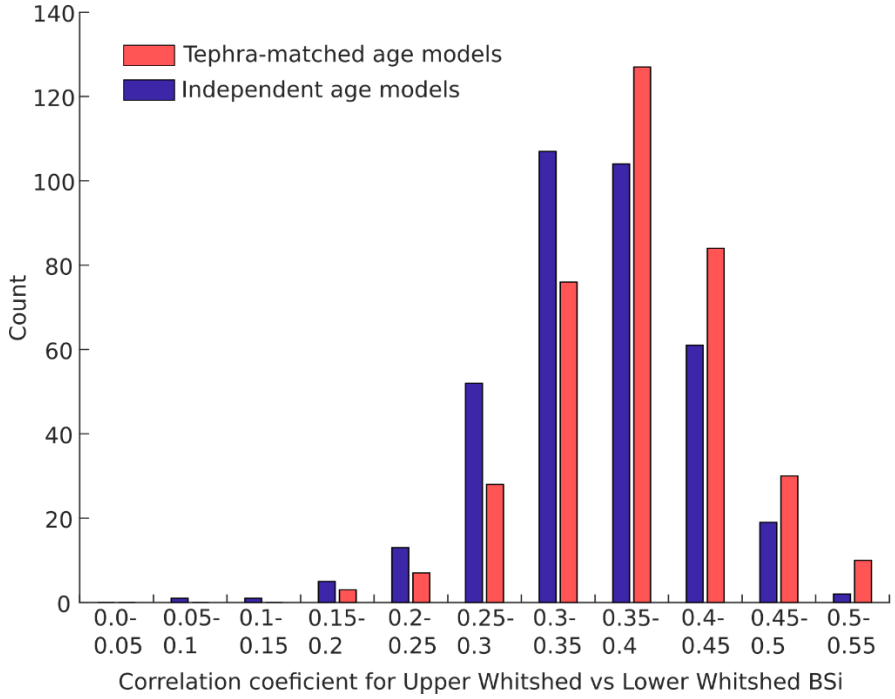

Fig. 7. Frequency of the correlation coefficients between the biogenic silica (BSi) time series from Upper and Lower Whitshed Lakes calculated for 365 age-ensemble members (details on the BSi data are in Zander, 2015). Blue and red bars compare the independent age-model outputs with the tephra-matched outputs, respectively. The tephra-matched age models tend to yield better correlations between the BSi records of the two lakes.

508 The tephra-matching method used in this study could potentially be improved through more
509 complete integration into the Bayesian process of the *Bacon* modeling software. The *ad hoc*
510 method used in this study reduces the number of members from the age ensemble, and cannot
511 inform the estimates of parameters in the models, thus losing the possibility of incorporating
512 Bayesian learning in the estimates of the distribution of sedimentation rates and their
513 autocorrelation. Nevertheless, given the small changes to the age model overall, the differences
514 between our *ad hoc* method and formal integration are likely negligible.
515
516 *4.2. Tephras*
517 Correlating tephras between sedimentary sequences requires multiple criteria, none of which
518 alone is absolutely conclusive. By using MS profiles, physical characteristics and major-oxide
519 geochemistry, correlations can be made with reasonable confidence, but many challenges exist.
520 Of the 11 beds sampled for geochemical analysis, only four were visible on the core face. The
521 use of crypotephra increases the potential to incorporate material from multiple eruptions,
522 including reworked tephra grains, and therefore may introduce greater uncertainty, especially
523 when the number of recovered grains is small. Several of the samples from the Whitshed Lakes
524 exhibit widely scattered geochemical data, which casts some uncertainty on the geochemical
525 correlations. For instance, 11-UW-2-163.5 (CU1157, 5863 ± 229 BP) and 10-WS-2-189
526 (CU1150, 5498 ± 291 BP) contain scattered geochemical data without a strong similarity
527 coefficient. Both samples contain a low-silica mode (59-69% silica) and high-silica mode (75-
528 80% silica). Primarily lower-silica grains were measured from 11-UW-2-163.5, and primarily
529 higher-silica grains were measured in 10-WS-2-189. Despite these differences, the geochemical

data overlap (Fig. 5), and do not rule out the correlation of these samples based on the unique and distinctive MS profiles found in the cores from both the Whitshed Lakes (Fig. 8).

These samples highlight some of the challenges that accompany the use of crytotephra for tephrochronological studies. The discrepancies in geochemistry we found in these samples could be caused by one of the following possible reasons. (1) Stratification of the composition of a disseminated tephra deposit within several centimeters of sediment, which would not be fully captured by our 1-cm-thick samples centered on the highest MS value. (2) Different depositional conditions at the core sites of the two lakes (e.g. differing flow regimes affecting sorting by particle size or density). (3) Fractionation effects when preparing tephra samples for analysis (e.g. during heavy liquid separation), or sampling bias in the selection of grains to analyze. (4) The samples contain tephra from multiple eruptions, which are represented in different proportions at the two lakes. If this is the case, it does not necessarily mean that it is incorrect to consider these depths as time synchronous. The spikes in MS mark zones of higher concentrations of tephra and possibly other minerogenic material within the sediment. Even if the tephra grains are reworked, an event such as a flood or earthquake could have caused the deposition of these layers of higher MS at the same time in both lakes.

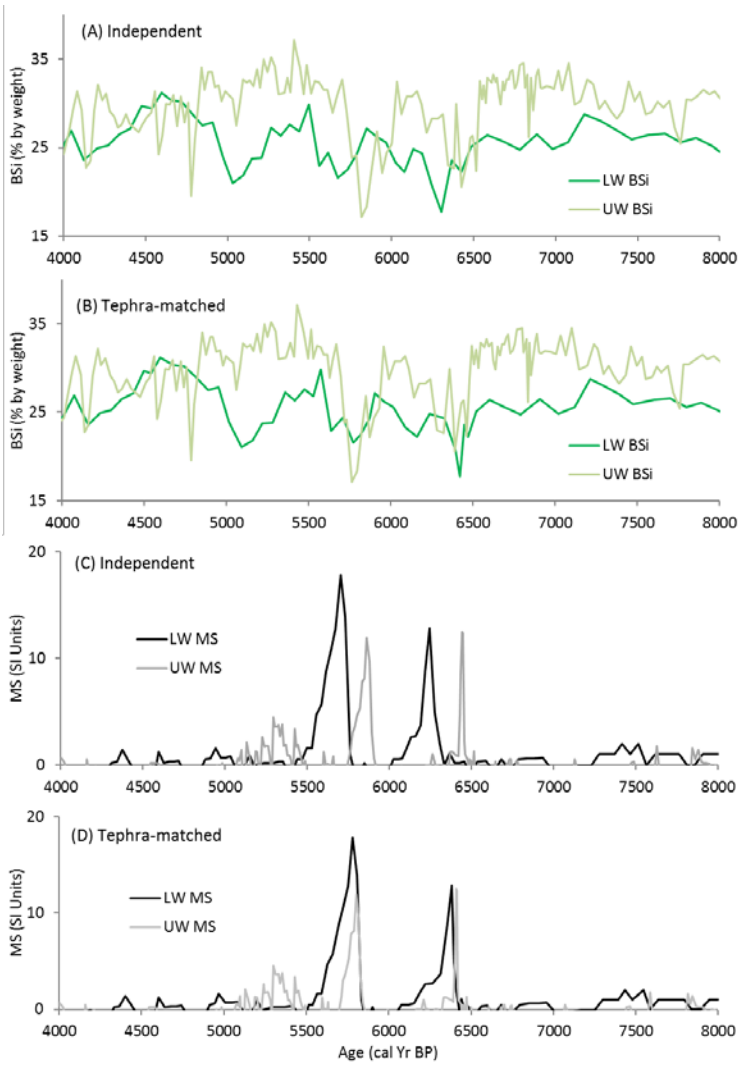

546

547 **Fig. 8.** Example of synchronization using tephra-matching techniques for two proxy time series
548 over the time period 4000-8000 cal yr BP. (A) Biogenic silica (BSi) data from both lakes plotted
549 using ages derived from the independent age models. (B) The same BSi data plotted using the
550 tephra-matched age models. (C) Magnetic susceptibility (MS) data from both lakes plotted using
551 the independent age models. (D) The same MS data plotted using the tephra-matched age
552 models. These spikes in MS represent zones of disseminated cryptotephra that are assumed to be
553 time equivalent (samples 10-WS-2-189, 11-UW-2-163.5, 10-WS-2-198.5 and 11-UW-2-2-185).

554

555 The fact that every tephra found in Lower Whitshed Lake was also found in Upper Whitshed
556 Lake provides some confidence that MS spikes provide a reliable indicator of tephra in our study
557 lakes. Two tephra samples may correlate with samples taken from Cabin Lake (Zander et al.,
558 2013), just 26 km away; however, the 95% confidence intervals do not overlap, suggesting either
559 an age bias, or multiple eruptions with very similar geochemistry. If there is an age bias, the
560 Cabin Lake chronology is more likely to be in error because the age models from the Whitshed
561 Lakes yield overlapping ages for each correlated tephra.
562 Two samples were taken from depths without major MS spikes, with the goal of locating
563 tephra from the 1912 CE eruption of Novarupta, which could be a useful time marker. Payne and
564 Symeonakis (2012) suggest the Cordova area likely received distal tephra fallout from the
565 eruption, but this fallout would not have been of significant thickness as the source is about 570
566 km away. The sample (11-UW-2A-5) closest in age to this eruption yielded only a single grain of
567 1912 Novarupta-like composition. Similarly, MS failed to locate tephra from this eruption at
568 Cabin Lake (Zander et al., 2013). Novarupta ash has not yet been detected in the near-surface
569 sediment from three lakes with high sedimentation rates in the Cook Inlet region, much closer to
570 the source volcano (Boes et al., in press). Additional non-visible tephra deposits that are not
571 represented by a prominent MS peak are likely present in the Whitshed Lake cores, as indicated
572 by the presence of numerous shards in sample 11-UW-2A-2.5, which was taken from an area of
573 relatively low MS. MS is a useful tool for locating tephra deposits (de Fontaine et al., 2007), but
574 even in sediments with very low background MS, it is possible for tephra material to be
575 undetected by MS.
576 Overall, the glass chemistries are indicative of AAAP (Type I) sources (Fig. S2). Attribution
577 to specific eruptions from individual volcanoes is more difficult due to ambiguities in ages,

similarities in composition between multiple events from the same source, and incomplete proximal eruption records. On the basis of the geochemical criteria presented by Zander et al. (2013), samples 11-UW-2-185 and 10-WS-2-198.5 are most likely from Augustine volcano, although the specific eruption is unclear. Samples 11-UW-2A-13 and 10-WS-2-104.5 contain andesitic glass that is geochemically similar to material erupted from Crater Peak on Mount Spurr (the only Cook Inlet volcano known to produce andesitic glass). However, the SC values make this source determination somewhat uncertain (SC = 0.80 when these samples are compared to Crater Peak 1953 sample AT252A, USGS Alaska Tephra Lab; Zander et al., 2013). The beds represented by 11-UW-2A-36.5 and 10-WS-2-127.5 and by 11-UW-2-355 have chemistries suggestive of Redoubt or Iliamna volcanoes, but it is not possible to refine this further without additional data. The rest of the samples are from unidentified AAAP sources.

Tephra deposits in lakes constitute important records of volcanic events, their ages, and their distribution, in part because lacustrine tephra deposits have much greater preservation potential than proximal deposits on volcano slopes and because age modeling of lacustrine sequences can provide robust tephra ages. The tephrostratigraphy from the Whitshed Lakes (in conjunction with Cabin Lake) will provide a framework for those emerging from other lake and marine sediments in the region, and as the number of records increases, our understanding of the volcanic events will improve.

5. Summary and Conclusions

Seven tephra deposits were located in Upper Whitshed Lake, and four in Lower Whitshed Lake. Four tephras were correlated between the lakes using the stratigraphic position and magnitude of MS peaks, major-oxide glass geochemistry, and ages derived from radiocarbon

samples. Bayesian age models were produced for each lake using the program *Bacon 2.2* and were based primarily on radiocarbon ages and supplemented by radioisotope profiles in the upper most portions of the stratigraphic sequences. The correlated tephras show that the independent radiocarbon-based age models for the two lakes are in close agreement because the 95% confidence intervals overlap for all four correlated markers.

A novel approach was used to synchronize the two records using four correlated tephras. MATLAB code was developed to select those ensemble members from the *Bacon* model output with age estimates of the correlated tephra that agree within 25 years. This method narrowed the confidence intervals of the age models by about 3%, and strengthened the best age estimate for the four correlated tephras. This technique may be useful for other studies that aim to synchronize multiple dated records with confident stratigraphic correlations. The ages and compositions of the tephras reported here contribute to the regional tephrochronology and will be useful for future studies of similar aged deposits in the region.

Supporting Information

Additional supporting information can be found in the online version of this article:

https://doi.org/10.1016/j.quageo.2018.01.005

Table S1: ^{210}Pb, ^{137}Cs and ^{241}Am profiles from Upper Whitshed Lake

Table S2: $^{239+240}$Pu profiles from Upper and Lower Whitshed Lakes

Table S3: Upper Whitshed age model inputs

Table S4: Lower Whitshed age model inputs

Table S5: Complete analytical data on Whitshed Lakes tephra samples

Table S6: Upper Whitshed age model output

Table S7: Lower Whitshed age model output

Fig. S1: Tephra source differentiation - reference data

Fig. S2: Tephra source differentiation - Whitshed Lake data

Fig. S3: Independent age-model for Upper Whitshed Lake

Fig. S4: Independent age-model for Lower Whitshed Lake

Appendix: Tephra matching source code

Acknowledgements

R. Scott Anderson, Hannah Bailey, Katie Detrich and Joe Licciardi assisted in the field, and R. Scott Anderson, Michael Ketterer, John Southon, Katherine Whitacre, and Handong Yang provided supporting laboratory analysis. We thank Maarten Blaauw and Kristi Wallace for their helpful comments. This study was funded by the US National Science Foundation (EAR-0823522 and ARC-0909332). Eyak Corporation kindly allowed access to their land.

638 **References**

639 Appleby, PG, Oldfield, F, 1978. The calculation of ^{210}Pb dates assuming a constant rate of
640 supply of unsupported ^{210}Pb to the sediment. *Catena* 5, 1-8.

641 Blaauw, M, Christen, JA, 2011. Flexible paleoclimate age-depth models using an autoregressive
642 gamma process. *Bayesian Analysis* 6, 457-474.

643 Borchardt GA, Aruscavage PJ, Millard HT Jr. 1972. Correlation of the Bishop ash, a Pleistocene
644 marker bed, using instrument activation analysis. *Journal of Sedimentary Petrology* 42,
645 301-306.

646 Boes, E, Van Daele, M, Moernaut, J, Schmidt, S, Jensen BJL, Praet, N, Kaufman, D, Haeussler,
647 P, Loso, MG, De Batis, M, in press. Varve formation during the past three centuries in
648 three large proglacial lakes in south-central Alaska. *Geological Society of America*
649 *Bulletin*. doi: 10.1130/B31792.1

650 Burns, SJ, Fleitmann, D, Matter, A, Kramers, J, Al-Subbary, AA, 2003. Indian Ocean climate
651 and an absolute chronology over Dansgaard/Oeschger events 9 to 13. *Science* 301, 1365-
652 1367.

653 de Fontaine, CS, Kaufman, DS, Anderson, RS, Werner, A, Waythomas, CF, Brown, RA, 2007.
654 Late Quaternary distal tephra-fall deposits in lacustrine sediments, Kenai Peninsula,
655 Alaska. *Quaternary Research* 68, 64–78.

656 Fohlmeister, J, 2012. A statistical approach to construct composite climate records of dated
657 archives. *Quaternary Geochronology* 14, 48-56.

658 Garrett, E, Barlow, N, Cool, H, Kaufman, D, Shennan, I, et al., 2015. Constraints on regional
659 drivers of relative sea-level change around Cordova, Alaska. *Quaternary Science Reviews*
660 113, 48-59

661 Hildreth, W, 1987. New perspectives on the eruption of 1912 in the Valley of Ten Thousand
662 Smokes, Katmai National Park, Alaska. *Bulletin of Volcanology* 49, 680-693.
663 Hoek, WZ, Bohncke, SJP, 2001. Oxygen-isotope wiggle matching as a tool for synchronising
664 ice-core and terrestrial records over Termination 1. *Quaternary Science Reviews* 20,
665 1251-1264.
666 Howarth, JD, Fitzsimons, SJ, Jacobsen, GE, Vandergoes, MJ, Norris RJ, 2013. Identifying a
667 reliable target for radiocarbon dating sedimentary records from lakes. *Quaternary*
668 *Geochronology* 17, 68-80
669 Kaufman, DS, Jensen, BJ, Reyes, AV, Schiff, CJ, Froese, DG, et al., 2012. Late Quaternary
670 tephrostratigraphy, Ahklun Mountains, SW Alaska. *Journal of Quaternary Science* 27,
671 344-359.
672 Ketterer ME, Hafer KM, Jones VJ, Appleby, PG, 2004. Rapid dating of recent sediments in Loch
673 Ness: inductively coupled plasma mass spectrometric measurements of global fallout
674 plutonium. *Science of the Total Environment* 322, 221–229.
675 Krawiec, AC, Kaufman, DS, Vaillencourt, DA, 2013. Age models and tephrostratigraphy from
676 two lakes on Adak Island, Alaska. *Quaternary Geochronology* 18, 41-53.
677 Kuehn SC, Froese DG, 2010. Tephra from ice – A simple method to routinely mount, polish, and
678 quantitatively analyze sparse fine particles. *Microscopy and Microanalysis* 16, 218–225.
679 Lowe, DJ, 2011. Tephrochronology and its application: a review. *Quaternary Geochronology* 6,
680 107-153.
681 Marwan, N, Thiel, M, Nowaczyk, NR, 2002. Cross recurrence plot based synchronization of
682 time series. *Nonlinear Processes in Geophysics* 9, 325-331.

683 Payne RJ, Symeonakis E, 2012. The spatial extent of tephra deposition and environmental
684 impacts from the 1912 Novarupta eruption. *Bulletin of Volcanology* 74, 2449-2458.
685 Preece SJ, Westgate JA, Gorton MP, 1992. Compositional variation and provenance of late
686 Cenozoic distal tephra beds, Fairbanks area, Alaska. *Quaternary International* 13/14: 97–
687 101.
688 Plafker, G, 1969. Tectonics of the March 27, 1964 Alaska Earthquake. *U.S. Geological Survey*
689 *Professional Paper 543–I.*
690 Reimer, PJ, Bard, E, Bayliss, A, Beck, JW, Blackwell, PG, et al., 2013. IntCal13 and Marine13
691 radiocarbon age calibration curves 0-50,000 yr cal BP. *Radiocarbon* 55, 1869-1887.
692 Zander, PD, 2015. Tephrochronology and paleoenvironmental change during the past 15,000
693 years at Whitshed Lakes, south-central Alaska, M.S. Thesis, Northern Arizona
694 University, 128 p.
695 Zander, PD, Kaufman, DS, Kuehn, SC, Wallace, KL, Anderson, RS, 2013. Early and late
696 Holocene glacial fluctuations and tephrostratigraphy, Cabin Lake, Alaska. *Journal of*
697 *Quaternary Science* 28, 761–771.